Engineering 3 (2017) 232–243

Contents lists available at ScienceDirect

Engineering

journal homepage: www.elsevier.com/locate/eng

Research
Smart Process Manufacturing—Article

Improving Prediction Accuracy of a Rate-Based Model of an MEA-Based Carbon Capture Process for Large-Scale Commercial Deployment

Xiaobo Luo, Meihong Wang*

Department of Chemical and Biological Engineering, The University of Sheffield, Sheffield S1 3JD, UK

ARTICLE INFO

Article history:
Received 13 November 2016
Revised 17 January 2017
Accepted 30 January 2017
Available online 17 March 2017

Keywords:
Process modeling
Model validation
Monoethanolamine
Carbon capture
Combined cycle gas turbine power plant
Carbon capture and storage

ABSTRACT

Carbon capture and storage (CCS) technology will play a critical role in reducing anthropogenic carbon dioxide (CO_2) emission from fossil-fired power plants and other energy-intensive processes. However, the increment of energy cost caused by equipping a carbon capture process is the main barrier to its commercial deployment. To reduce the capital and operating costs of carbon capture, great efforts have been made to achieve optimal design and operation through process modeling, simulation, and optimization. Accurate models form an essential foundation for this purpose. This paper presents a study on developing a more accurate rate-based model in Aspen Plus® for the monoethanolamine (MEA)-based carbon capture process by multistage model validations. The modeling framework for this process was established first. The steady-state process model was then developed and validated at three stages, which included a thermodynamic model, physical properties calculations, and a process model at the pilot plant scale, covering a wide range of pressures, temperatures, and CO_2 loadings. The calculation correlations of liquid density and interfacial area were updated by coding Fortran subroutines in Aspen Plus®. The validation results show that the correlation combination for the thermodynamic model used in this study has higher accuracy than those of three other key publications and the model prediction of the process model has a good agreement with the pilot plant experimental data. A case study was carried out for carbon capture from a 250 MW_e combined cycle gas turbine (CCGT) power plant. Shorter packing height and lower specific duty were achieved using this accurate model.

1. Introduction

1.1. Background

Increasing concentrations of greenhouse gases (GHGs) caused by anthropogenic activities are responsible for most of global warming [1]. Carbon dioxide (CO_2) is a main GHG, accounting for 76% of total GHG emissions in 2010 [2]. The International Energy Agency (IEA) set up a BLUE Map scenario with 14 Gt of CO_2 emissions in 2050 compared with 57 Gt of CO_2 emissions in the baseline scenario [3]. In order to achieve this target, carbon capture and storage (CCS) technology will play a vital role in delivering 19% of cumulative CO_2 emission reductions between 2015 and 2050 in the power sector [3].

Among the three main approaches envisaged for CO_2 capture from power plants—pre-combustion capture, post-combustion capture, and oxyfuel capture [4]—the solvent-based post-combustion carbon capture (PCC) process is regarded as the most promising technology for commercial deployment [5,6]. In solvent-based carbon capture technology, CO_2 is separated from flue gas after combustion by chemical absorption; monoethanolamine (MEA) is regarded as a benchmark solvent for this process.

1.2. Previous studies

A complex electrolyte aqueous solvent is involved in the MEA-

* Corresponding author.
E-mail address: meihong.wang@sheffield.ac.uk

http://dx.doi.org/10.1016/J.ENG.2017.02.001

based PCC process [7], which requires accurate thermodynamic modeling and physical properties calculations for its modeling. Thermodynamic data, especially regarding CO_2 solubility, have been reported for 30 wt% MEA aqueous solutions [8,9] and for a wider MEA solution concentration range [10,11]. For the parameterization and validation of physical properties calculation methods of an MEA-H_2O-CO_2 mixture, experimental data on MEA aqueous solutions are valuable, especially with different CO_2 loading. Correlations for the calculation of the density and viscosity of MEA-H_2O-CO_2 mixtures at different temperatures and MEA concentrations can be found in the literature [12–14]. In terms of mass transfer and thermal performance of the integrated MEA-based PCC process, several experimental campaigns [15,16] have been conducted.

For a highly nonlinear electrolyte MEA-H_2O-CO_2 solution, the electrolyte non-random two-liquid (eNRTL) model [17,18] is the most widely adopted model [10,19]. Recently, some studies [20,21] have also used the perturbed-chain statistical association fluid theory (PC-SAFT) [22,23] equation of state (EOS) for the vapor phase of an MEA-H_2O-CO_2 mixture, with a system temperature of up to 500 K and a system pressure of up to 15 MPa.

For this capture process, significant energy is consumed for solvent regeneration [6]. Thus, the cost of carbon capture is high when PCC is added to the emitters. Great research efforts have been taken to reduce the carbon capture cost through process modeling and simulation approaches. Most early studies were carried out for the parametric sensitivity analysis of solvent-based PCC processes in the context of coal-fired power plants [24–27]. Some studies were carried out on integrations between power plants and carbon capture plants [28–30]. Several studies focused on optimizing the whole plant through process optimization [31–34].

However, obvious inconsistencies in the literature were found for key equipment design features and key operational variables. For example, the packing height varies from 13.6 m [35] to 30.6 m [32] for the absorber and from 7.6 m [35] to 28.15 m [21] for the stripper for similar capture tasks. The optimal lean loading range is equally wide from 0.132 $mol_{CO_2}{\cdot}mol^{-1}_{MEA}$ [31] to 0.234 $mol_{CO_2}{\cdot}mol^{-1}_{MEA}$ [36], with corresponding specific duty in a range from 3.77 $GJ{\cdot}t^{-1}_{CO_2}$ to 4.35 $GJ{\cdot}t^{-1}_{CO_2}$. Those inconsistencies cause confusion for future research in this field. They may also cause some trouble for the engineering design of a large-scale commercial deployment.

The main reasons for the abovementioned knowledge gaps may be related to conflicts between the complexity of the integrated system and the accuracy requirement of the modeling and simulation studies. Firstly, the models used in some publications were relatively simple. For example, equilibrium models were used for the mass transfer and reaction in both the absorber and the stripper [37]. For a rate-based model, the correlations for calculations of mass transfer coefficients, interfacial area, liquid holdup, and pressure drop inside packing beds also have a large impact on the prediction accuracy [38,39]. For the kinetics-controlled reactions, it is found that the values of the kinetics of reverse reactions for bicarbonate formation are different for the absorber and the stripper [40]. Inappropriate correlations used in the models would significantly affect the accuracy of model predictions.

1.3. Aim and novel contribution

In order to address the abovementioned knowledge gaps, this study aims to improve the accuracy of the rate-based model in Aspen Plus® for the MEA-based carbon capture process. The novel contributions of this paper can be justified by the following: ① A new combination of correlations was selected after comparing model predictions with the experimental vapor-liquid phase equilibrium (VLE) data; ② the correlations for predicting the liquid density of the mixture and the effective vapor-liquid interfacial area were improved by coding Fortan subroutines in Aspen Plus®; ③ different kinetics parameters were used for reverse reactions for bicarbonate formation in the absorber and the stripper, respectively, thus reflecting the nature of the different operating conditions in the absorber and the stripper; and ④ the rate-based process model was validated with the experimental data and pilot plant data at three different stages, including thermodynamic modeling, physical properties calculations, and process model development at the pilot scale.

2. Framework of modeling of the solvent-based carbon capture process

Using an amine solvent to absorb CO_2 from exhaust gases is a reactive absorption process involving an electrolyte aqueous solvent [6]. The modeling of this non-ideal multi-component system is a systematic work at different levels. Fig. 1 outlines the modeling framework for such a PCC process. Although the software package Aspen Plus® was used for the modeling and simulation of the process, it is important to check the calculation methods with their corrections in order to ensure the accuracy of the process simulation and optimization.

Accurate prediction of the physical properties of pure components and mixtures is one of the basic prerequisites in process modeling and simulation. As the first step, the thermodynamic model should be developed to present VLE and to calculate the state parameters of the MEA-H_2O-CO_2 mixture, such as the temperature, pressure, and composition of the liquid and vapor phases. The solubility of CO_2 in the MEA-H_2O-CO_2 mixture is a key parameter, and is normally used for validation purposes for the calibration of the correlations or for selection for VLE calculation.

The physical properties are part of the correlations for heat transfer, mass transfer, interfacial area, liquid holdup, and pressure drop. It is important to choose the right physical property models to ensure the success of process modeling and simulation.

At the process level, both absorption and desorption in the packed columns are key processes. A rate-based model offers better accuracy than an equilibrium model for the absorption performance of the columns [41]. This accuracy is a function of the appropriate correlations used for liquid and vapor phase mass transfer coefficients, the effective vapor-liquid interfacial area, and the pressure drop in the rate-based model.

This framework shows that the rate-based model for this solvent-based carbon capture process is a highly nonlinear model, which has numerous parameters, correlations, and equations. Therefore, it is not realistic to completely repeat the published models with the same input conditions. This is also the main consideration behind the choice to use three-stage validations in this study, and to update some correlations by coding a Fortran subroutine in Aspen Plus® to ensure model accuracy, rather than directly comparing the process performance with those of other published models. Using this three-stage model validation method, the model was dissected in detail based on the logical structure of numerical modeling, allowing more insights to be obtained.

3. Thermodynamic modeling of the MEA-H_2O-CO_2 system

3.1. EOSs and relevant model parameters

In this study, the PC-SAFT EOS [22,23] is used to calculate the properties of the vapor phase, and the eNRTL [18] method is used to model the electrolyte system of an MEA-H_2O-CO_2 mixture.

3.1.1. The PC-SAFT EOS for the vapor phase

Compared with some typical cubic EOSs such as the Peng-Robinson

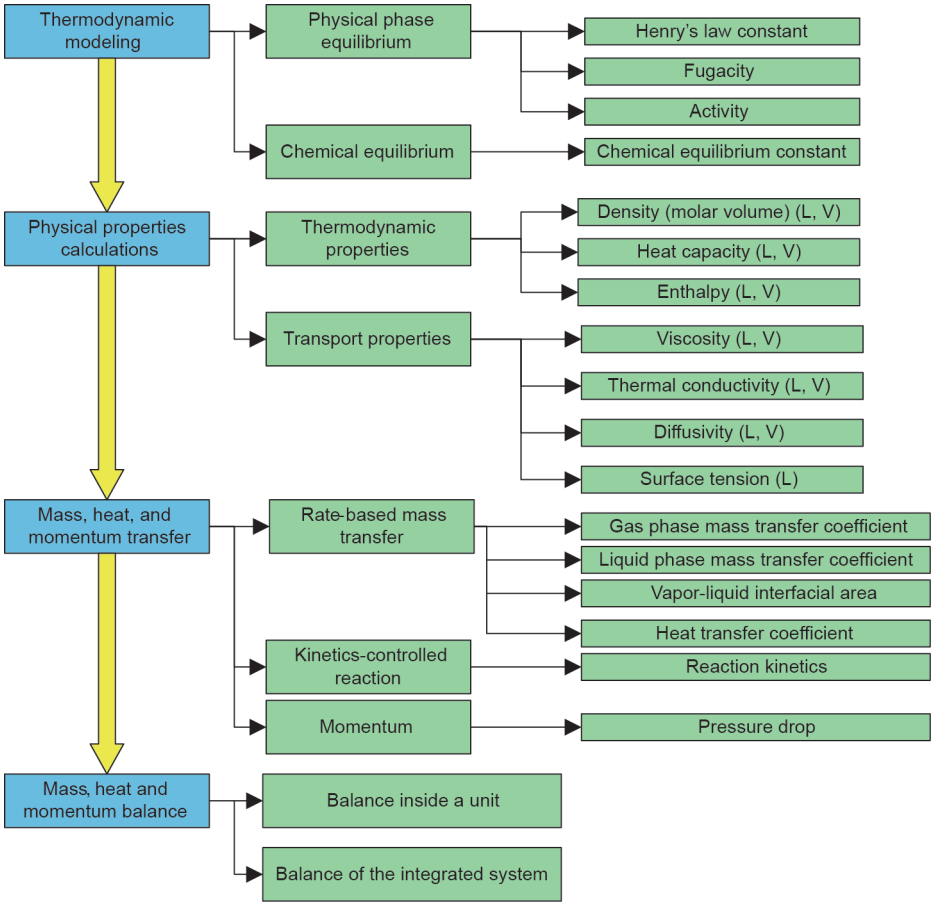

Fig. 1. Framework of the modeling of a solvent-based PCC process. L: liquid phase; V: vapor phase.

(PR) EOS and the Soave-Redlich-Kwong (SRK) EOS, the PC-SAFT EOS is able to accurately estimate vapor phase fugacity coefficients at high pressures [20,42], which is important for accurate performance predictions of CO_2 compression with an outlet pressure as high as 136 bar[†] [43]. Table 1 [20,23,44] summarizes the PC-SAFT parameters of pure components, and Table 2 [45,46] lists the binary interaction parameters (k_{ij}) of MEA-H_2O and CO_2-H_2O.

3.1.2. The eNRTL method for the liquid phase

The liquid phase of an MEA-H_2O-CO_2 mixture is a typical electrolyte solution [19]. The eNRTL method has been validated and used to model electrolyte solutions in many publications [19,20,27,40,47].

Table 3 [20,44,46] summarizes the model parameters used for this study, and their sources. Most of the parameters were obtained from the SRK-ASPEN databank [44], and some were updated by recent studies by regression using new experimental data [46].

Table 1
PC-SAFT parameters of pure components.

Component	H_2O	CO_2	MEA
Source	[23]	[44]	[20]
Segment number parameter, m	1.0656	2.5692	2.9029
Segment energy parameter, ε	366.51 K	152.1 K	306.2 K
Segment size parameter, σ	3.0007 Å	2.5637 Å	3.1067 Å
Association energy parameter, ε^{AB}	2500.7 K	0 K	2369 K
Association volume parameter, K^{AB}	0.034868 Å^3	0 Å^3	0.01903 Å^3

3.2. Physical solubility and Henry's law constant

Physical solubility is the equilibrium between CO_2 molecules in the vapor phase and those in liquid solutions; it is calculated using

Table 2
Binary parameters for the PC-SAFT EOS.

Component pairs	MEA-H_2O	CO_2-H_2O
Source	[45]	[46]
k_{ij}	−0.052	0

Table 3
Model parameters for eNRTL.

Model parameters	Component	Source
Antoine equation parameters	MEA	[44]
$\Delta_{vap}H$	MEA	[44]
Dielectric constant	MEA	[44]
NRTL binary parameters	CO_2-H_2O binary	[46]
	MEA-H_2O binary	[20]
	Molecule-electrolyte binaries	[20]
$\Delta_f G^{ig}_{298.15}$, $\Delta_f H^{ig}_{298.15}$, C^{ig}_p	H_2O, MEA, CO_2	[44]
$\Delta_f G^{\infty,aq}_{298.15}$, $\Delta_f H^{\infty,aq}_{298.15}$	H_3O^+, HCO_3^-, CO_3^{2-}, OH^-	[44]
	$MEAH^+$, $MEACOO^-$	[20]
$C^{\infty,aq}_p$	H_3O^+, OH^-	[44]

[†] 1 bar = 10^5 Pa.

Henry's law. The Henry's law constants for CO_2 with water and with MEA are required, and can be calculated using Eq. (1):

$$\ln\left(H_{i-j}\right) = C_1 + \frac{C_2}{T} + C_3 \ln T + C_4 T \quad (1)$$

where H_{i-j} is the binary Henry's law constant between pure components i and j; T is the system temperature; and C_1, C_2, C_3, and C_4 are correlations for Henry's law constants. Table 4 [46,47] summarizes the available binary Henry's law constants for an MEA-H_2O-CO_2 mixture. For the system of an MEA-H_2O-CO_2 mixture, most publications only take gas components such as CO_2 and N_2 as Henry components. In addition, most studies only consider Henry's law constants for CO_2 with H_2O [19]. The Henry's law constants for CO_2 with H_2O have been well studied by Yan and Chen [46] by examining extensive quantities of experimental VLE data for the CO_2-H_2O binary system. Liu et al. [47] considered Henry's law constants for CO_2 with MEA.

3.3. Chemical reaction equilibrium

Liquid phase chemical reactions involved in the MEA-H_2O-CO_2 system can be expressed as follows:

R1: water dissociation

$$2H_2O \rightleftharpoons H_3O^+ + OH^-$$

R2: dissociation of CO_2

$$CO_2 + 2H_2O \rightleftharpoons H_3O^+ + HCO_3^-$$

R3: dissociation of carbonate

$$HCO_3^- + H_2O \rightleftharpoons H_3O^+ + CO_3^{2-}$$

R4: dissociation of the protonated amine

$$MEAH^+ + H_2O \rightleftharpoons H_3O^+ + MEA$$

R5: carbonate formation

$$MEACOO^- + H_2O \rightleftharpoons HCO_3^- + MEA$$

The chemical equilibrium constants of these reactions were calculated using Eq. (2), and the related correlations are shown in Table 5 [19,48,49].

$$\ln K_j = C_1 + \frac{C_2}{T} + C_3 \ln T + C_4 T \quad (2)$$

where K_j refers to the chemical equilibrium constants for each reaction j; T is the system temperature; and C_1, C_2, C_3, and C_4 are correlations for the chemical equilibrium constants.

Once the chemical equilibrium constants are determined, the chemical equilibrium of each reaction is determined using Eq. (3) [19].

$$K_j = \left[\frac{\prod_{\text{reactant},i}\left(x_i\gamma_i\right)^{\nu_i}}{\prod_{\text{product},n}\left(x_n\gamma_n\right)^{\nu_n}}\right] \quad (3)$$

where i denotes the reactant component; n denotes the product component; x denotes the model fraction of each component in the liquid phase based on true species, molecular and ionic; γ denotes the activity coefficient; and ν denotes the stoichiometric coefficient of each component in reaction j.

3.4. Validation of CO_2 solubility prediction

3.4.1. Case setup

In order to compare and select appropriate correlations for this study, several combinations of correlations [19,20,47] were chosen for carrying out the validation against the experimental data. Table 6 [19,20,46,47,50,51] provides the model details.

3.4.2. Validation results

For model validation purposes, the model predictions were compared with the experimental data in terms of the CO_2 partial pressure and/or total pressure in the vapor phase for different CO_2 loading in an MEA aqueous solution. In this study, the experimental data from Ref. [11] were chosen because these data cover a wider range

Table 4
Correlations for the calculation of Henry's law constants (on the molality scale).

Component pairs	CO_2-H_2O	CO_2-MEA
Sources	[46]	[47]
C_1	100.650	89.452
C_2	−6147.7	−2934.6
C_3	−10.191	−11.592
C_4	0	0.01644
T (K)	273–473	280–600

Table 5
Correlations for chemical equilibrium constants (on the molality scale).

Reaction	C_1	C_2	C_3	C_4	T (°C)	Source
R1	132.8990	−13445.90	−22.4773	0	0–225	[48]
R2	231.4650	−12092.10	−36.7816	0	0–225	[48]
R3	216.0490	−12431.70	−35.4819	0	0–225	[48]
R4	−4.9074	−6166.12	0	−0.00098482	0–50	[49]
R5	2.8898	−3635.09	0	0	25–120	[19]

Table 6
Different combinations of correlations for validation.

	This study	Zhang et al. [20]	Liu et al. [47]	Austgen et al. [19]
EOS for vapor	PC-SAFT	PC-SAFT	SRK	SRK
EOS for liquid	eNRTL	eNRTL	eNRTL	eNRTL
Dielectric constants	Zhang et al. [20]	Zhang et al. [20]	Ikada et al. [50]	Ikada et al. [50]
NRTL binary	Zhang et al. [20]	Zhang et al. [20]	Liu et al. [47]	Austgen et al. [19]
Electron pair	Zhang et al. [20]	Zhang et al. [20]	Liu et al. [47]	Austgen et al. [19]
Henry's law constants (CO_2 in H_2O)	Yan and Chen [46]	Yan and Chen [46]	Chen et al. [51]	Chen et al. [51]
Henry's law constants (CO_2 in MEA)	Liu et al. [47]	Zhang et al. [20]	Liu et al. [47]	—
Chemical equilibrium constants	Liu et al. [47]	Zhang et al. [20]	Liu et al. [47]	Austgen et al. [19]

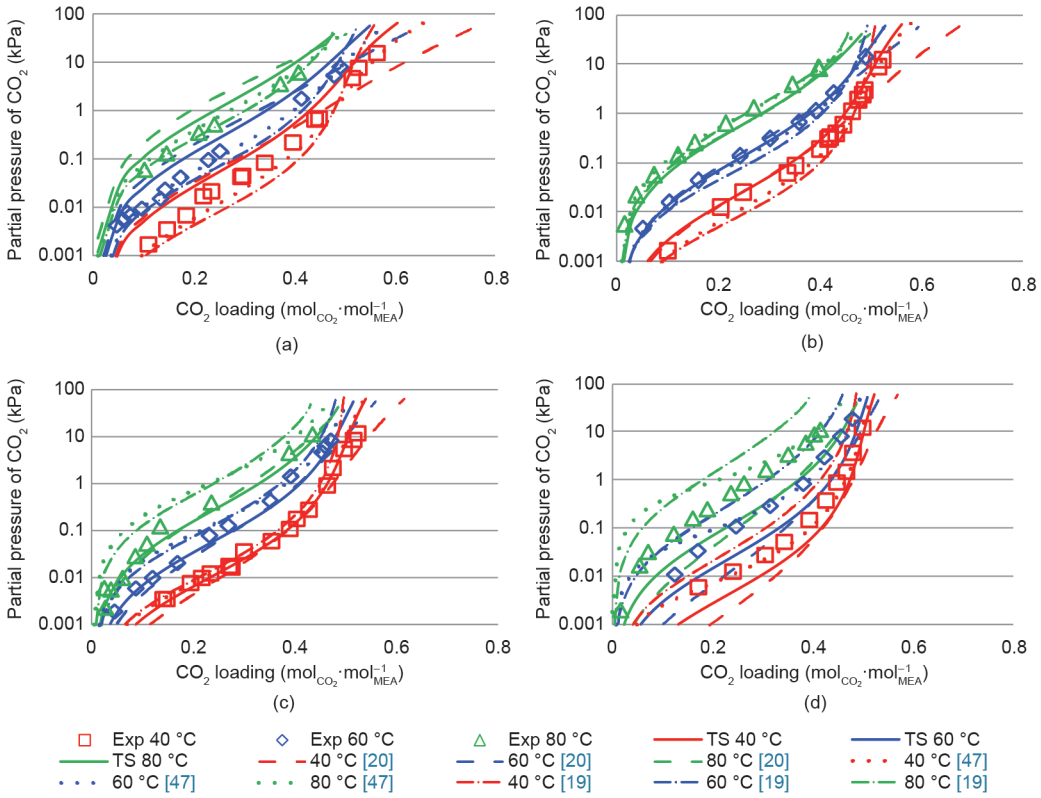

Fig. 2. CO_2 partial pressure as a function of CO_2 loading with: (a) 15 wt% MEA solvent, (b) 30 wt% MEA solvent, (c) 45 wt% MEA solvent, and (d) 60 wt% MEA solvent. Exp: experimental data; TS: this study.

Table 7
MAPE of validation with CO_2 partial pressure of the MEA-H_2O-CO_2 system.

	This study	Zhang et al. [20]	Liu et al. [47]	Austgen et al. [19]
15 wt% MEA	23.86%	43.33%	7.97%	11.06%
30 wt% MEA	7.63%	6.09%	6.40%	8.72%
45 wt% MEA	10.62%	11.57%	38.76%	36.47%
60 wt% MEA	17.97%	20.86%	61.90%	51.56%
Average	15.02%	20.46%	28.76%	26.95%

of MEA concentrations than other publications, as well as wider ranges of system temperatures and pressures.

Fig. 2 depicts comparisons between model predictions and experimental data for the partial pressure of CO_2 in the vapor phase of MEA-H_2O-CO_2 mixtures for different concentrations of MEA. Table 7 [19,20,47] presents the mean absolute percentage error (MAPE) of validation results at different MEA concentrations. Generally, the deviations between experimental data and model predictions become bigger at the lower (15 wt%) and higher (45 wt%–60 wt%) MEA concentrations, compared with the 30 wt% MEA concentration. It is noticeable that the model predictions of this study at 15 wt% concentration are worse than those of Ref. [47]. The reason is that some of the correlations used in this study were inherited from Ref. [20]. Furthermore, none of these four combinations produced good predictions that covered low to high MEA concentrations, which reflects an inherent limitation of the correlation method: A correlation should not go beyond the conditions of the data for its regression. However, most of existing correlations that were used for the thermodynamic modeling of the MEA-H_2O-CO_2 system were regressed based on experimental data at 30 wt% MEA concentration solvent.

4. Physical properties of the MEA-H_2O-CO_2 system

4.1. Physical property model

The physical properties include: ① thermodynamic properties, such as density, enthalpy, and heat capacity; and ② transport properties, such as viscosity, surface tension, thermal conductivity, and diffusivity. Table 8 lists the chosen models for the property calculation for the mixture in this study. It should be noted that the correlations for the density of the liquid mixture are obtained from Ref. [14] by coding a Fortran subroutine in Aspen Plus®.

4.2. Available experimental data for validation

Table 9 [14,52–54] provides the available experimental data from the literature for the physical properties validation of MEA-H_2O-CO_2. The vapor phase of the MEA-H_2O-CO_2 mixture under the operating temperature (20–150 °C) and pressure (1–2 bar) of the absorber and stripper is not an issue, and no experimental data are available for those properties of the vapor phase. Available experimental data for the thermal conductivity of the liquid phase were not currently found. Furthermore, direct measurement of CO_2 diffusivity in an MEA aqueous solution is impossible because CO_2 reacts with MEA. The NO_2 analogy method was used to produce the data for CO_2 diffusivity [55].

4.3. Validation results

Fig. 3 and Fig. 4 present comparisons between the model predictions and the experimental data for different properties of the MEA-H_2O-CO_2 mixture at different concentrations of MEA.

Table 10 presents the deviations of the validation results for the physical properties plotted in Fig. 3 and Fig. 4. Both MAPE and the

Table 8
Correlations used for the property calculation of the mixture.

	Property	Phase	Correlation
Thermodynamic properties	Density	Liquid	Han et al. [14]
		Vapor	PC-SAFT
	Enthalpy	Liquid	eNRTL
		Vapor	PC-SAFT
	Heat capacity	Liquid	Calculated from enthalpy
		Vapor	Calculated from enthalpy
Transport properties	Viscosity	Liquid	Jones-Dole
		Vapor	Chapman-Enskog-Brokaw
	Diffusivity	Liquid (molecule)	Wilke-Chang
		Liquid (ion)	Nernst-Hartly
		Vapor	Dawsom-Khoury-Kobayashi
	Thermal conductivity	Liquid	Sato-Reidel
		Vapor	Stiel-Thodos
	Surface tension	Liquid	Hakim-Steinberg-Stiel

Table 9
Available experimental data for the physical properties of the liquid phase.

Property	Process conditions of the experimental data			Source of experimental data
	Temperature (°C)	MEA concentration (wt%)	CO_2 loading ($mol_{CO_2}·mol^{-1}_{MEA}$)	
Density	25–140	30, 40, 50, 60	0.1–0.6	[14]
Heat capacity	25	10, 20, 30, 40	0–0.5	[52]
Viscosity	25	10, 20, 30, 40	0–0.5	[53]
Surface tension	25	10, 20, 30, 40	0–0.5	[54]

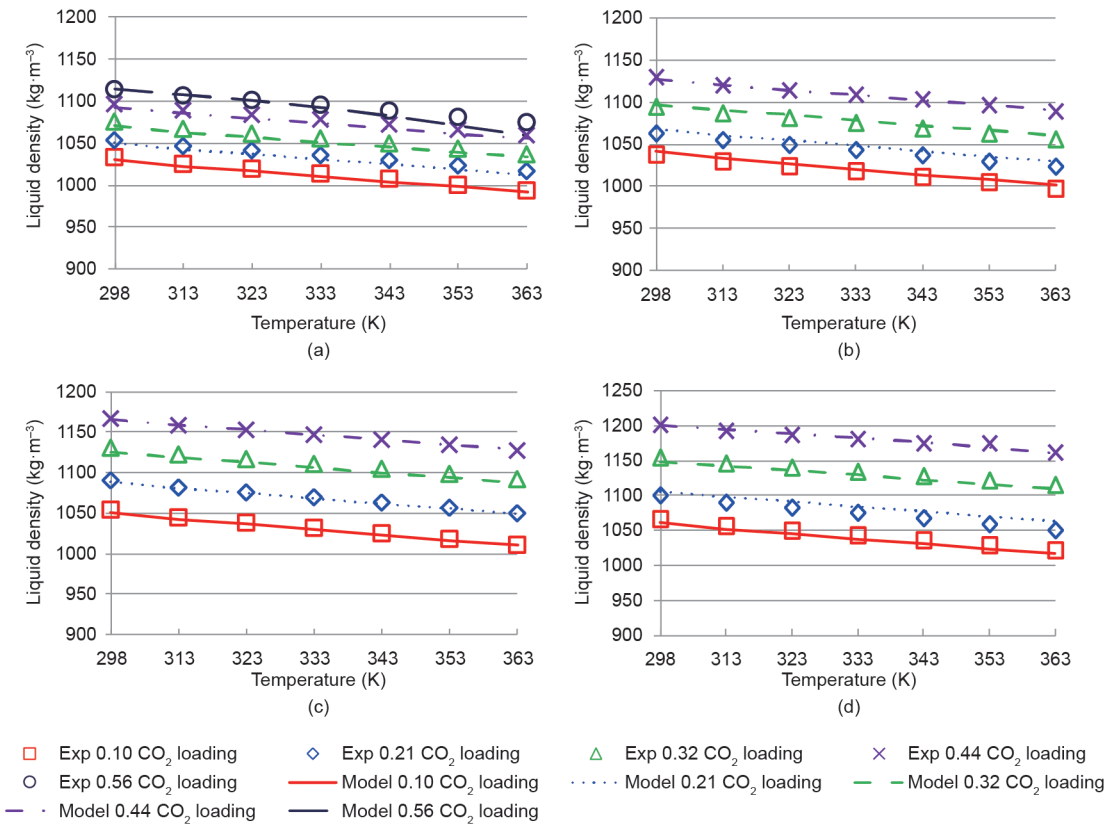

Fig. 3. Liquid density of MEA-H_2O-CO_2 with different CO_2 loading ($mol_{CO_2}·mol^{-1}_{MEA}$) at: (a) 30 wt% MEA solvent, (b) 40 wt% MEA solvent, (c) 50 wt% MEA solvent, and (d) 60 wt% MEA solvent. Model: model predictions.

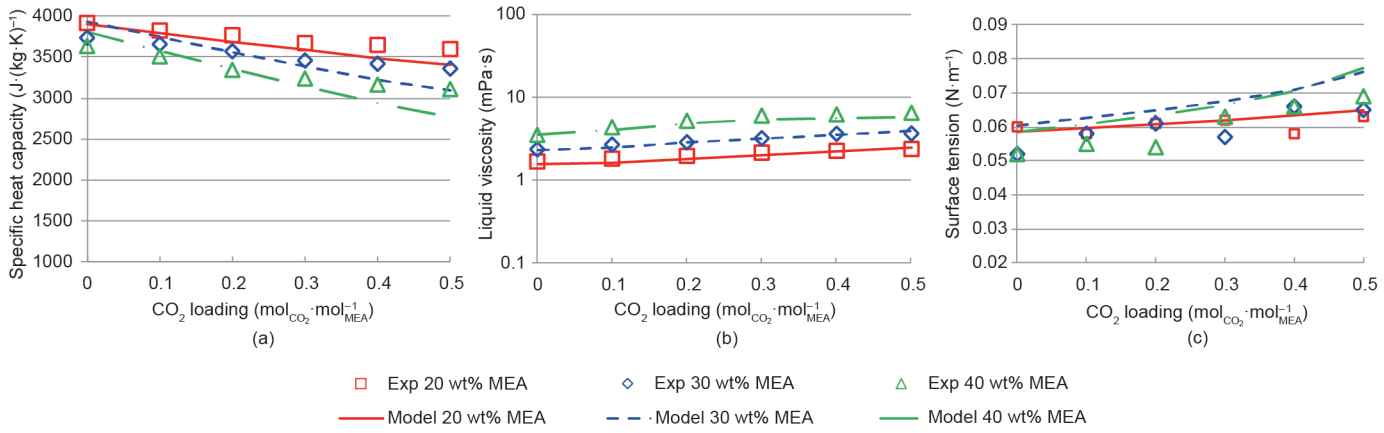

Fig. 4. Physical properties of MEA-H_2O-CO_2 at different MEA concentrations and 298.15 K for: (a) specific heat capacity, (b) liquid viscosity, and (c) surface tension.

Table 10
Deviations of the model predictions from the experimental data.

Property	MAPE (%)	Max APE (%)
Density	0.348	1.480
Specific heat capacity	3.74	10.74
Viscosity	5.46	9.70
Surface tension	8.58	18.29

maximum absolute percentage error (APE) are given. For the liquid density, the model predictions are in good agreement with the experimental data over the full range of system conditions. For the specific heat capacity (Fig. 4(a)), the deviations gradually increase as CO_2 loading rises. For the surface tension, the experimental data themselves have large deviations (Fig. 4(c)).

5. Process model development and validation at the pilot scale

5.1. Introduction of the pilot plant

In this study, the pilot plant located at the University of Kaiserslautern [56] was chosen for model validation, for the following reasons: ① Both the absorber and the stripper use Mellapak 250Y packing, which is regarded as appropriate structured packing for industrial deployment [57]; and ② the experimental data are comprehensive and well presented in the publications from this plant [16], which enables more comprehensive validation that can be compared with other studies. Table 11 summarizes the equipment features and the ranges of the key operation variables. (For more details about this pilot plant, refer to Ref. [16].)

Table 11
Main specifications of the pilot plant.

Main specifications		Parameter
Flue gas source		Natural gas burner
Flue gas flow rate ($kg·h^{-1}$)		30–100
CO_2 concentration in the flue gas (mol%)		3–14
Solvent flow rate ($kg·h^{-1}$)		50–350
MEA mass fraction in the CO_2-free solvent ($kg_{MEA}·kg_{H_2O}^{-1}$)		0.1–0.3
CO_2 loading in the lean solvent ($mol_{CO_2}·mol_{MEA}^{-1}$)		0.1–0.32
Temperature of cooling water (°C)		5–10
Absorber	Diameter (m)	0.125
	Height of packing (m)	4.2
	Packing type	Structured packing Mellapak 250Y
	Operating pressure (bar)	Atmospheric pressure
	Operating temperature (°C)	40–70
Stripper	Diameter (m)	0.125
	Height of packing (m)	2.52
	Packing type	Structured packing Mellapak 250Y
	Operating pressure (bar)	1–2.5
	Operating temperature (°C)	100–130

5.2. Process model development

5.2.1. Model flowsheet and process description

Fig. 5 shows the flowsheet of this steady-state process model in Aspen Plus®. The flue gas leaving the power plant goes to a gas blower and is then cooled to 40–50 °C before entering the absorber, in order to improve the absorption efficiency [25]. The scrubbed flue gas is emitted to the atmosphere and the CO_2-rich solvent is discharged from the bottom of the absorber and enters the stripper. The CO_2-rich solvent is regenerated inside the stripper with heat input to the reboiler. The regenerated solvent is cooled and re-circulated to the absorber for reuse.

5.2.2. Kinetics-controlled reactions

In Section 3.3, the equilibrium reactions of the MEA-H_2O-CO_2 mixture were described during the thermodynamic modeling. In the rate-based model, the reaction of dissociation of CO_2 and the reaction of carbonate formation should be considered as kinetics-controlled reactions [27]:

R2*: dissociation of CO_2

$$CO_2 + 2H_2O \longrightarrow H_3O^+ + HCO_3^-$$

$$H_3O^+ + HCO_3^- \longrightarrow CO_2 + 2H_2O$$

R5*: carbonate formation

$$MEACOO^- + H_2O \longrightarrow HCO_3^- + MEA$$

$$HCO_3^- + MEA \longrightarrow MEACOO^- + H_2O$$

Power law expressions were used for the kinetics-controlled reactions. The reaction rates of reactions R2* and R5* can be calculated by Eq. (4) [27].

$$r_j = k_j^o T^n \exp\left(-\frac{E_j}{RT}\right)\prod_{i=1}^{N} C_i^{\alpha_{ij}} \quad (4)$$

where r_j is the reaction rate for reaction j in $mol·(min·m^3)^{-1}$; k_j^o is the

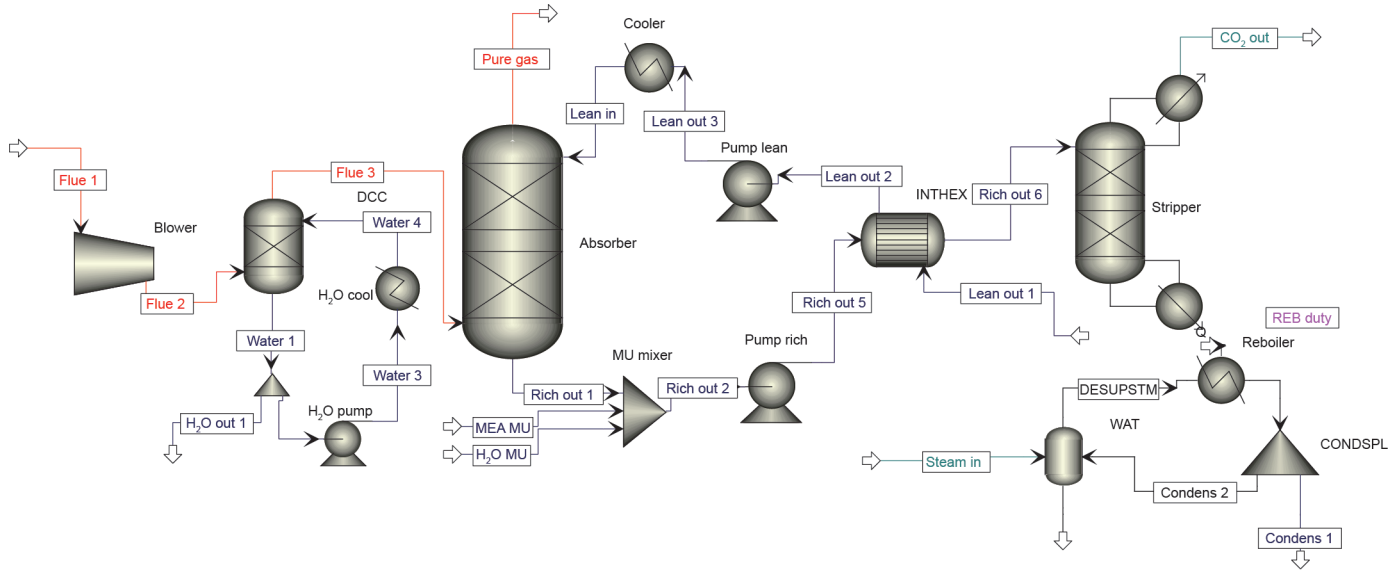

Fig. 5. Process flowsheet in Aspen Plus®. MU: make up; REB: reboiler; CONDSPL: condensate splitter; DESUPSTM: desuperheater steam; INTHEX: internal heat exchanger; DCC: direct contact cooler; WAT: water desuperheater.

pre-exponential factor in kmol·(m^3·s)$^{-1}$; T is the system temperature in K; n is the temperature factor; E_j is the activation energy in kJ·mol^{-1}; R is the gas constant; C_i is the mole fraction of species i; and α_{ij} is the reaction order of component i in reaction j. k_j^o and E_j for the reactions were calculated using the experimental data shown in Table 12 [40].

5.2.3. Rate-based mass transfer

The modeling of the absorber and the stripper was based on two-film theory [58], which is used to describe the mass transfer of components between the gas phase and the liquid phase. According to two-film theory, a vapor film and liquid film with a phase equilibrium interface are assumed between the bulk gas and bulk liquid phases. Chemical reactions are assumed to occur in the liquid film only.

For the RateSep model in Aspen Plus®, Zhang et al. [27] provided very detailed discussions about correlations and settings. In this study, the VPlug flow model was chosen in order to model the bulk properties with reasonable accuracy, since the "Countercurrent" model sometimes causes oscillations in the temperature profile even though it is the closest approximation of the real situation [59]. It was also noted that the discretization points of the liquid film need to be over 10, in order to achieve accuracy; otherwise, the simulation results may exhibit over-predictions of the rate of mass transfer.

For the correlations related to mass transfer, Razi et al. [59] validated 12 correlation combinations with experimental data from the CO_2 enhanced separation and recovery (CESAR) pilot data; the results show that Billet and Schultes [60] give an accurate correlation. Table 13 [59–62] lists the parameters and correlations related to mass transfer that were used in this study. Here, a Fortran subroutine was used to implement the correlation of Ref. [61] for the calculation of interfacial area.

Table 12
Parameters k_j^o and E_j in Eq. (4) [40].

Related species	Reaction direction	k_j^o (kmol·(m^3·s)$^{-1}$)	E_j (kJ·mol^{-1})
$MEACOO^-$	Forward	3.02×10^{10}	41.20
	Reverse (absorber)	5.52×10^{23}	69.05
	Reverse (stripper)	6.56×10^{27}	95.24
HCO^{3-}	Forward	1.33×10^{17}	55.38
	Reverse	6.63×10^{16}	107.24

5.3. Model validation

For the MEA-based carbon capture process, the key operational parameters affecting performance are the CO_2 concentration in the flue gas, the MEA concentration in the solvents, the lean loading, and the liquid-to-gas (L/G) ratio. Thus, four sets of experiments from Ref. [16] were chosen for model validation purposes. These include: ① Experiments A1–A6, with different CO_2 concentrations in the flue gases; ② Experiments A24–A27, with different MEA concentrations at two different CO_2 concentrations in the flue gases; ③ Experiments A28–A33, with different solvent flow rates at high CO_2 concentrations in the flue gases; and ④ Experiments A34–A39, with different solvent flow rates at low CO_2 concentrations in the flue gases. Model validations were carried out based on the same feed conditions, and the CO_2 loading in the lean solvent (lean loading) was targeted by varying the reboiler duty of the stripper. Experimental data and model predictions for CO_2 loading in a rich solvent (rich loading), the CO_2 capture level, and the stripper reboiler duty could then be compared.

Fig. 6 illustrates the bias between experimental data and model predictions for CO_2 capture level, rich loading, and specific duty under the same input conditions. The validation results for CO_2 capture level and rich loading show a good agreement. Regarding the specific duty, reboiler duty in the experiments was affected by heat loss from the equipment and pipelines, which could not be measured directly. Although the values for specific duty provided in Ref. [16] were corrected, the deviations themselves could not be evaluated, which may be the reason for high APEs for the validation results of the specific duty. MAPEs of the model predictions for the CO_2

Table 13
Parameters and correlations selection for mass transfer in the RateSep model.

Parameters	Correlations
Flow model	VPlug [59]
Film discretization points	20 [59]
Mass transfer coefficients	See Ref. [60]
Interfacial area	See Ref. [61]
Liquid holdup	See Ref. [60]
Heat transfer coefficient	See Ref. [62]
Pressure drop	Sulzer correlation

capture level, the stripper reboiler duty, and the rich CO_2 loading, as compared with the experimental data from Ref. [16], are 1.78%, 1.54%, and 7.49%, respectively.

Validations were also conducted to compare the temperature profiles and the CO_2 composition profiles inside the absorber and the stripper based on Experiments A1, A2, and A3 [16]. CO_2 concentrations in the flue gases are 8.5 mol% for A1, 16.5 mol% for A2, and 5.5 mol% for A3. Fig. 7 shows that the model predictions are in very good agreement with the experimental data. One statement is that the total packing height is 2.25 m inside the stripper; the 3 m position of the packing in Fig. 7(b) and Fig. 7(d) represents the reboiler of the stripper. The comparison results show that the model predictions are in very good agreement with the experimental data.

6. Case study

6.1. Methodology for model scale-up from pilot scale to commercial scale

To match the capacity requirement of handling the flue gas from power plants at an industry scale, the model of the carbon capture process at a pilot scale was scaled up, based on chemical engineering principles regarding the estimation of column diameter and pressure drop [63].

As initial inputs to the process model at an industrial scale in Aspen Plus®, first-guess diameters are required for both the absorber and the stripper. The column diameters can be calculated from the maximum flooding vapor. In this study, a generalized pressure drop correlation (GPDC) figure (Fig. 8) [64] was used to estimate the maximum flooding vapor. The abscissa and ordinate are presented in Eq. (5) and Eq. (6) [64], respectively.

$$F_{LV} = \frac{L_W^*}{V_W^*}\sqrt{\frac{\rho_V}{\rho_L}} \tag{5}$$

$$K_4 = \frac{13\left(V_W^*\right)^2 F_P\left(\mu_L/\rho_L\right)^{0.1}}{\rho_V\left(\rho_L-\rho_V\right)} \tag{6}$$

In Eq. (5), F_{LV} is a flow parameter. For the absorber, the liquid feed

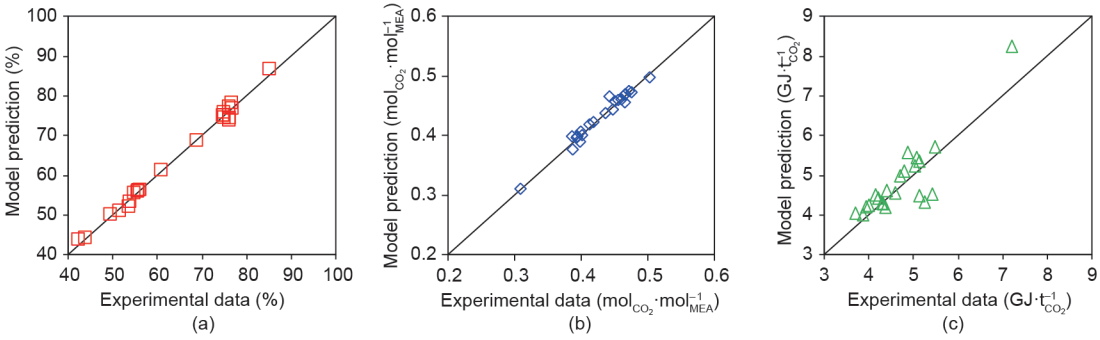

Fig. 6. The bias between experimental data and model prediction for: (a) CO_2 capture level, (b) rich loading, and (c) specific duty.

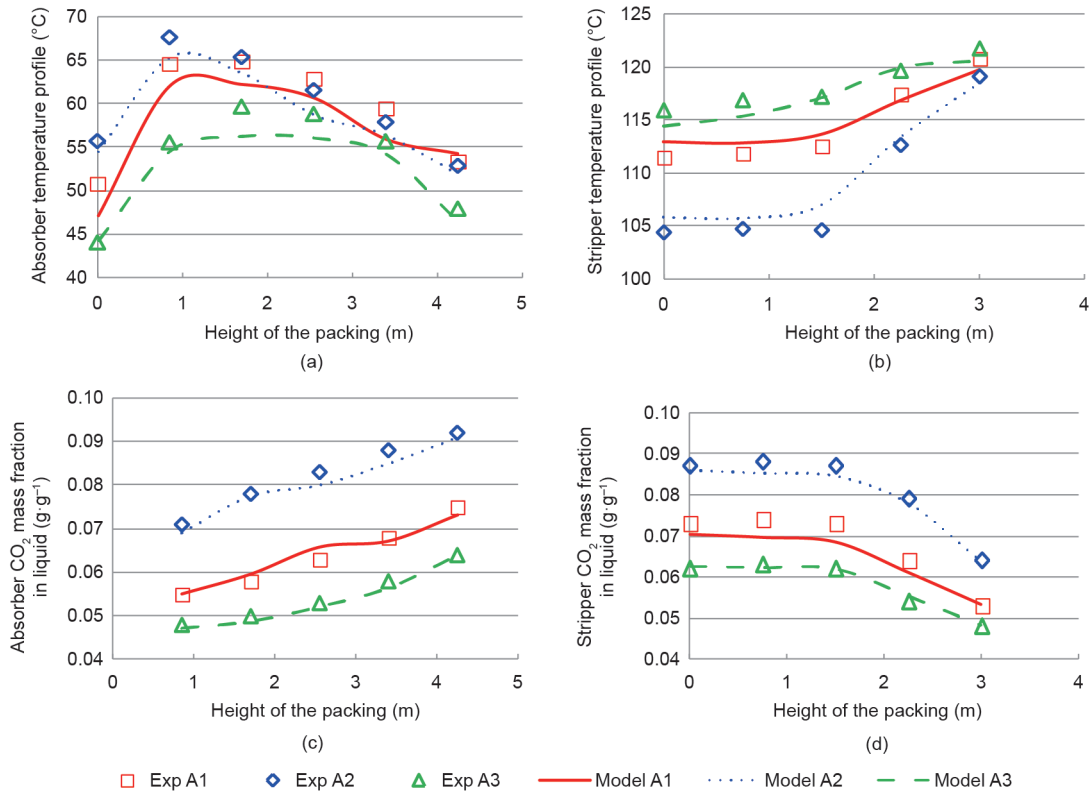

Fig. 7. Validation results between model predictions and experimental data. (a) Temperature profile of the absorber; (b) temperature profile of the stripper; (c) CO_2 composition profile inside the absorber; (d) CO_2 composition profile inside the stripper.

is the lean solvent. Its flow rate can be estimated using Eq. (7) [21].

$$F_{\text{Lean}} = \frac{F_{\text{Flue}} x_{\text{CO}_2} \psi_{\text{CO}_2}}{100(\alpha_{\text{Rich}} - \alpha_{\text{Lean}})} \left[\frac{M_{\text{MEA}}}{44.009} \left(1 + \frac{1 - \omega_{\text{MEA}}}{\omega_{\text{MEA}}} \right) + \alpha_{\text{Lean}} \right] \quad (7)$$

where F_{Lean} is the mass flow rate of the lean solution; F_{Flue} is the mass flow rate of the flue gas; x_{CO_2} is the mass fraction of CO_2 in the flue gas; ψ_{CO_2} is the required carbon capture level; M_{MEA} is the molar weight of MEA; α_{Rich} and α_{Lean} are the CO_2 loading ($\text{mol}_{\text{CO}_2}\cdot\text{mol}^{-1}_{\text{MEA}}$) in rich solvent and lean solvent, respectively; and ω_{MEA} is the MEA mass fraction in solvent.

From Eq. (6) , V^*_{W} (vapor mass flow rate per unit cross-sectional area) is calculated; next, the total cross-sectional area can be obtained given the flue gas flow rate. In this equation, K_4 is a load parameter obtained from Fig. 8, according to the value of F_{LV} and the specified pressure drop; F_{P} is a packing factor.

In order to achieve good liquid and gas distribution and to avoid flooding inside packing beds, a pressure drop of 15–50 mmH_2O[†] per meter of packing for absorber and stripper was recommended [64]. In this study, a maximum pressure drop per unit height of 20.83 mmH_2O [65] was used, considering the formation of the MEA solvent [21]. It should be noted that the design of the column internals, such as gas/liquid distributors and re-distributors, is crucial in order to ensure good gas and liquid distribution inside the absorber and regenerator for such large diameters.

6.2. Carbon capture from a 250 MW_e CCGT power plant

In this case study, the carbon capture plant was scaled up to handle the flue gas from the 250 MW_e combined cycle gas turbine (CCGT) power plant described in Ref. [66]. For comparison purposes, the input conditions of the flue gas and the operating conditions of the columns were chosen to be same as for the case without exhaust gas recirculation (EGR) in Ref. [66]; these conditions are presented in Table 14.

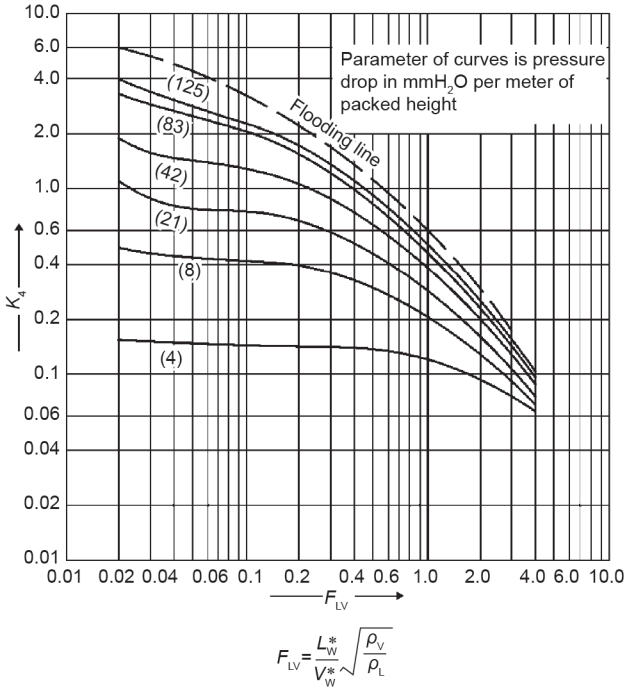

Fig. 8. Generalized pressure drop correlation [64].

It is noticeable that the upper limit of the pressure drop per height of packing bed is 42 mmH_2O in Ref. [66]; at this value, the columns may have serious flooding [21]. In this case study, the flooding factors of the columns were set up to 65%. Another consideration is that structured packing is preferred for a large-diameter absorption column, due to the possibility of serious mal-distribution of both the liquid and vapor phases inside the random packing bed [67]. Therefore, Mellapak 250Y packing, which is regarded as an appropriately structured packing type for industrial deployment [57], was chosen for the packing beds inside the absorber and the stripper in this case study.

The first-guess diameters of the absorber and the stripper can be calculated using the method presented in Section 6.1. Starting from that point, these parameters were simulated using the improved rate-based model developed in Aspen Plus®. Table 15 summarizes a comparison of the results of this study with those presented by Canepa et al. [66], in terms of equipment size and process parameters. It shows that the design of this study achieved smaller equipment size and lower thermal duty.

One significant difference is that the packing heights in both the absorber and the stripper in this study are significantly smaller than those in Ref. [66]. One contributor is that higher efficiency structured packing was used in this study, which allows a lower height of transfer unit (HTU); the total packing height was then reduced, while keeping the same number of transfer units (NTU). At the same time, using the more accurate model provides more confidence in the simulation results, such that a conservative margin may not be needed. After all, capture levels reached as high as 90%–95% during experiments with short packing beds for both the absorber and the stripper of the pilot plants. In the experimental study by Dugas [15], the packing heights of both the absorber (with IMTP No. 40 random packing) and the stripper (with Flexipac 1Y) are 6.1 m. Notz et al. [16] reported the packing heights of the absorber and the stripper (with Mallepak 250Y) to be 4.2 m and 2.25 m, respectively, for their pilot plant.

It is also noticeable that the specific duty in this study is lower than that in Ref. [66]. The results in Table 15 show that the rich loading of this study is slightly higher, which may reflect the impact of thermodynamic modeling. With the same CO_2 concentration in the flue gas, the solubility of CO_2 that is calculated by this improved thermodynamic model may be slightly higher when close to its saturation. This situation also results in a smaller flow rate of the solvent entering the stripper. Thus, the heat requirement for solvent evaporation in the stripper decreases. At the same time, using more

Table 14
Boundary conditions of the solvent-based PCC process.

Description	Value
Flue gas flow rate ($\text{kg}\cdot\text{s}^{-1}$)	356
Composition (mass fraction)	N_2: 0.863; H_2O: 0.046; CO_2: 0.076; Ar: 0.015
Flue gas temperature (°C)	40
Solvent MEA content (wt%)	32.5
Lean solvent temperature (°C)	40
Capture level (%)	90
Columns flooding (%)	65
Operating pressure of the absorber (bar)	1.01
Operating pressure of the stripper (bar)	1.62

[†] 1 mmH_2O = 9.8066136 Pa.

Table 15
Comparison results between this study and the literature.

Description	This study	Canepa et al. [66]
Column diameter of the absorber (m)	14.0	2 × 9.5[a]
Packing height of the absorber (m)	15.0	30.0
Column diameter of the striper (m)	6.0	8.2
Packing height of the stripper (m)	9.4	30.0
L/G ratio ($kg \cdot kg^{-1}$)	1.58	2.02
Lean solvent flow rate ($kg \cdot s^{-1}$)	563.91	720.46
Lean loading ($mol_{CO_2} \cdot mol_{MEA}^{-1}$)	0.303	0.300
Rich loading ($mol_{CO_2} \cdot mol_{MEA}^{-1}$)	0.472	0.456
Reboiler duty (MW_{th})	91.53	121.00
Reboiler temperature (°C)	114.16	117.00
Specific duty ($GJ \cdot t_{CO_2}^{-1}$)	3.76	4.97

[a] Two columns with same diameter of 9.5 m.

accurate kinetics for the reactions inside both the absorber and the stripper could also have a large impact on the predictions of heat requirement for solvent regeneration, although it is hard to dissect those highly nonlinear relations between those factors.

7. Conclusions

This paper presented a study on the development of an accurate rate-based steady-state model in Aspen Plus®, with some elements implemented in Fortran subroutines, for the MEA-based carbon capture process, along with a case study using this model. It was found that the correlations of the thermodynamic model have a significant impact on the prediction accuracy of the VLE of the MEA-H_2O-CO_2 mixture. A new combination of correlations was selected in this study, and shows better prediction performance. Following this step, the model from Ref. [14] was used, by coding a Fortran subroutine in order to improve the prediction accuracy of the liquid mixture density. The rate-based process model was improved by setting different kinetics for the reverse carbonate formation reactions in the absorber and the stripper, respectively, and by coding a Fortran subroutine for the effective gas-liquid interfacial area using the model from Ref. [61]. The model validation results show that the model predictions appear to be in good agreement with the experimental data from the pilot plant.

Using this accurate model, a case study was carried out for carbon capture fitted to a 250 MW_e CCGT power plant. The results show that this study achieved smaller equipment size and lower energy consumption than the previous study; these results may translate into significant savings in both capital investment and utility cost for the carbon capture plant.

Acknowledgement

This work was supported by the EU FP7 Marie Curie International Research Staff Exchange Scheme (PIRSES-GA-2013-612230).

Compliance with ethics guidelines

Xiaobo Luo and Meihong Wang declare that they have no conflict of interest or financial conflicts to disclose.

Nomenclature

C Correlations for property calculations
E_j Activation energy
F_p Packing factor
F_{LV} Flow parameter
H Henry's law constant
k_j^o The pre-exponential factor
K_j Chemical equilibrium constants of reaction j
L Total liquid flow rate in mass
P Pressure
R Ideal gas constant
r_j Reaction rate of reaction j
T Temperature
V Total vapor flow rate in mass
V_W^* Vapor mass flow rate per unit cross-sectional area
x Liquid-phase model fraction based on true species, molecular and ionic
y Vapor-phase mole fraction

Greek Letters

α CO_2 loading in lean solvent or rich solvent
α_{ij} Reaction order of component i in reaction j
ρ Density
ψ_{CO_2} CO_2 capture level
ω_{MEA} MEA mass fraction in solvent
γ Activity coefficient
v Stoichiometric coefficient of each component in reactions

Superscripts

o Standard state

Subscripts

CO_2 CO_2 component
Flue Flue gas
Lean Lean solvent
L Liquid phase
MEA Monoethanolamine
V Vapor phase
i Reactant component
j Chemical reaction
n Product component

References

[1] Pachauri RK, Allen MR, Barros VR, Broome J, Cramer W, Christ R, et al. Climate change 2014: Synthesis report. Contribution of Working Groups I, II and III to the Fifth Assessment Report of the Intergovernmental Panel on Climate Change. Core Writing Team, Pachauri RK, Meyer LA, editors. Geneva: Intergovernmental Panel on Climate Change; 2015 [cited 2016 Jun 6]. Available from: http://www.ipcc.ch/report/ar5/syr.
[2] Intergovernmental Panel on Climate Change. Climate change 2014: Mitigation of climate change. Working Group III contribution to the IPCC Fifth Assessment Report. Cambridge: Cambridge University Press; 2015.
[3] International Energy Agency. Energy technology perspectives 2010: Scenarios and strategies to 2050. Paris: OECD Publishing; 2010.
[4] Kanniche M, Gros-Bonnivard R, Jaud P, Valle-Marcos J, Amann JM, Bouallou C. Pre-combustion, post-combustion and oxy-combustion in thermal power plant for CO_2 capture. Appl Therm Eng 2010;30(1):53–62.
[5] Wang M, Lawal A, Stephenson P, Sidders J, Ramshaw C. Post-combustion CO_2 capture with chemical absorption: A state-of-the-art review. Chem Eng Res Des 2011;89(9):1609–24.
[6] Rochelle GT. Amine scrubbing for CO_2 capture. Science 2009;325(5948):1652–4.
[7] Kenig EY, Schneider R, Górak A. Reactive absorption: Optimal process design via optimal modeling. Chem Eng Sci 2001;56(2):343–50.
[8] Harris F, Kurnia KA, Mutalib MIA, Thanapalan M. Solubilities of carbon dioxide and densities of aqueous sodium glycinate solutions before and after CO_2 absorption. J Chem Eng Data 2009;54(1):144–7.
[9] Tong D, Trusler JPM, Maitland GC, Gibbins J, Fennell PS. Solubility of carbon dioxide in aqueous solution of monoethanolamine or 2-amino-2-methyl-1-propanol: Experimental measurements and modeling. Int J Greenh Gas Con 2012;6:37–47.
[10] Hilliard MD. A predictive thermodynamic model for an aqueous blend of potassium carbonate, piperazine, and monoethanolamine for carbon dioxide capture from flue gas [dissertation]. Austin: University of Texas at Austin; 2008.
[11] Aronu UE, Gondal S, Hessen ET, Haug-Warberg T, Hartono A, Hoff KA, et al. Solubility of CO_2 in 15, 30, 45 and 60 mass% MEA from 40 to 120 °C and model representation using the extended UNIQUAC framework. Chem Eng Sci 2011;66(24):6393–406.
[12] Cheng S, Meisen A, Chakma A. Predict amine solution properties accurately.

Hydrocarbon Process 1996;75(2):81–4.
[13] Hartono A, Mba EO, Svendsen HF. Physical properties of partially CO_2 loaded aqueous monoethanolamine (MEA). J Chem Eng Data 2014;59(6):1808–16.
[14] Han J, Jin J, Eimer DA, Melaaen MC. Density of water (1) + monoethanolamine (2) + CO_2 (3) from (298.15 to 413.15) K and surface tension of water (1) + monoethanolamine (2) from (303.15 to 333.15) K. J Chem Eng Data 2012;57(4):1095–103.
[15] Dugas RE. Pilot plant study of carbon dioxide capture by aqueous monoethanolamine [dissertation]. Austin: University of Texas at Austin; 2006.
[16] Notz R, Mangalapally HP, Hasse H. Post combustion CO_2 capture by reactive absorption: Pilot plant description and results of systematic studies with MEA. Int J Greenh Gas Con 2012;6:84–112.
[17] Song JH, Yoon JH, Lee H, Lee KH. Solubility of carbon dioxide in monoethanolamine + ethylene glycol + water and monoethanolamine + poly(ethylene glycol) + water. J Chem Eng Data 1996;41(3):497–9.
[18] Chen CC, Evans LB. A local composition model for the excess Gibbs energy of aqueous electrolyte systems. AIChE J 1986;32(3):444–54.
[19] Austgen DM, Rochelle GT, Peng X, Chen CC. Model of vapor-liquid equilibria for aqueous acid gas-alkanolamine systems using the electrolyte-NRTL equation. Ind Eng Chem Res 1989;28(7):1060–73.
[20] Zhang Y, Que H, Chen CC. Thermodynamic modeling for CO_2 absorption in aqueous MEA solution with electrolyte NRTL model. Fluid Phase Equilibr 2011;311:67–75.
[21] Agbonghae EO, Hughes KJ, Ingham DB, Ma L, Pourkashanian M. Optimal process design of commercial-scale amine-based CO_2 capture plants. Ind Eng Chem Res 2014;53(38):14815–29.
[22] Gross J, Sadowski G. Perturbed-chain SAFT: An equation of state based on a perturbation theory for chain molecules. Ind Eng Chem Res 2001;40(4):1244–60.
[23] Gross J, Sadowski G. Application of the perturbed-chain SAFT equation of state to associating systems. Ind Eng Chem Res 2002;41(22):5510–5.
[24] Abu-Zahra MRM, Schneiders LHJ, Niederer JPM, Feron PHM, Versteeg GF. CO_2 capture from power plants: Part I. A parametric study of the technical performance based on monoethanolamine. Int J Greenh Gas Con 2007;1(1):37–46.
[25] Kvamsdal HM, Haugen G, Svendsen HF. Flue-gas cooling in post-combustion capture plants. Chem Eng Res Des 2011;89(9):1544–52.
[26] Lawal A, Wang M, Stephenson P, Obi O. Demonstrating full-scale post-combustion CO_2 capture for coal-fired power plants through dynamic modeling and simulation. Fuel 2012;101:115–28.
[27] Zhang Y, Chen H, Chen CC, Plaza JM, Dugas R, Rochelle GT. Rate-based process modeling study of CO_2 capture with aqueous monoethanolamine solution. Ind Eng Chem Res 2009;48(20):9233–46.
[28] Lucquiaud M, Gibbins J. Retrofitting CO_2 capture ready fossil plants with post-combustion capture. Part 1: Requirements for supercritical pulverized coal plants using solvent-based flue gas scrubbing. P I Mech Eng A–J Pow 2009;223(3):213–26.
[29] Luo X, Wang M, Chen J. Heat integration of natural gas combined cycle power plant integrated with post-combustion CO_2 capture and compression. Fuel 2015;151:110–7.
[30] Liu X, Chen J, Luo X, Wang M, Meng H. Study on heat integration of supercritical coal-fired power plant with post-combustion CO_2 capture process through process simulation. Fuel 2015;158:625–33.
[31] Sipöcz N, Tobiesen FA. Natural gas combined cycle power plants with CO_2 capture—Opportunities to reduce cost. Int J Greenh Gas Con 2012;7:98–106.
[32] Mores PL, Godoy E, Mussati SF, Scenna NJ. A NGCC power plant with a CO_2 post-combustion capture option. Optimal economics for different generation/capture goals. Chem Eng Res Des 2014;92(7):1329–53.
[33] Luo X, Wang M. Optimal operation of MEA-based post-combustion carbon capture for natural gas combined cycle power plants under different market conditions. Int J Greenh Gas Con 2016;48(Part 2):312–20.
[34] Mac Dowell N, Shah N. Identification of the cost-optimal degree of CO_2 capture: An optimisation study using dynamic process models. Int J Greenh Gas Con 2013;13:44–58.
[35] Kvamsdal HM, Hetland J, Haugen G, Svendsen HF, Major F, Kårstad V, et al. Maintaining a neutral water balance in a 450 MW_e NGCC-CCS power system with post-combustion carbon dioxide capture aimed at offshore operation. Int J Greenh Gas Con 2010;4(4):613–22.
[36] Biliyok C, Canepa R, Wang M, Yeung H. Techno-economic analysis of a natural gas combined cycle power plant with CO_2 capture. In: Kraslawski A, Turunen I, editors Computer aided chemical engineering: The 23rd European Symposium on Computer Aided Process Engineering. Oxford: Elsevier; 2013. p. 187–92.
[37] Abu-Zahra MRM, Niederer JPM, Feron PHM, Versteeg GF. CO_2 capture from power plants: Part II. A parametric study of the economical performance based on mono-ethanolamine. Int J Greenh Gas Con 2007;1(2):135–42.
[38] Kvamsdal HM, Chikukwa A, Hillestad M, Zakeri A, Einbu A. A comparison of different parameter correlation models and the validation of an MEA-based absorber model. Energ Procedia 2011;4:1526–33.
[39] Razi N, Bolland O, Svendsen H. Review of design correlations for CO_2 absorption into MEA using structured packings. Int J Greenh Gas Con 2012;9:193–219.
[40] Zhang Y, Chen CC. Modeling CO_2 absorption and desorption by aqueous monoethanolamine solution with aspen rate-based model. Energ Procedia 2013;37:1584–96.
[41] Lawal A, Wang M, Stephenson P, Yeung H. Dynamic modelling of CO_2 absorption for post combustion capture in coal-fired power plants. Fuel 2009;88(12):2455–62.
[42] Zhang Y, Chen CC. Thermodynamic modeling for CO_2 absorption in aqueous MDEA solution with electrolyte NRTL model. Ind Eng Chem Res 2011;50(1):163–75.
[43] Luo X, Wang M, Oko E, Okezue C. Simulation-based techno-economic evaluation for optimal design of CO_2 transport pipeline network. Appl Energ 2014;132:610–20.
[44] Aspen Technology, Inc. Aspen physical property system: Physical property methods. Burlington: Aspen Technology, Inc.; 2013.
[45] Fakouri Baygi S, Pahlavanzadeh H. Application of the perturbed chain-SAFT equation of state for modeling CO_2 solubility in aqueous monoethanolamine solutions. Chem Eng Res Des 2015;93:789–99.
[46] Yan Y, Chen CC. Thermodynamic modeling of CO_2 solubility in aqueous solutions of NaCl and Na_2SO_4. J Supercrit Fluid 2010;55(2):623–34.
[47] Liu Y, Zhang L, Watanasiri S. Representing vapor-liquid equilibrium for an aqueous MEA-CO_2 system using the electrolyte nonrandom-two-liquid model. Ind Eng Chem Res 1999;38(5):2080–90.
[48] Edwards TJ, Maurer G, Newman J, Prausnitz JM. Vapor-liquid equilibria in multicomponent aqueous solutions of volatile weak electrolytes. AIChE J 1978;24(6):966–76.
[49] Bates RG, Pinching GD. Acidic dissociation constant and related thermodynamic quantities for monoethanolammonium ion in water from 0 °C to 50 °C. J Res Nat Bur Stand 1951;46(5):349–52.
[50] Ikada E, Hida Y, Okamoto H, Hagino J, Koizumi N. Dielectric properties of ethanolamines. Bull Inst Chem Res Kyoto Univ 1968;46(5):239–47.
[51] Chen CC, Britt HI, Boston JF, Evans LB. Extension and application of the pitzer equation for vapor-liquid equilibrium of aqueous electrolyte systems with molecular solutes. AIChE J 1979;25(5):820–31.
[52] Weiland RH, Dingman JC, Cronin DB. Heat capacity of aqueous monoethanolamine, diethanolamine, *N*-methyldiethanolamine, and *N*-methyldiethanolamine-based blends with carbon dioxide. J Chem Eng Data 1997;42(5):1004–6.
[53] Weiland RH, Dingman JC, Cronin DB, Browning GJ. Density and viscosity of some partially carbonated aqueous alkanolamine solutions and their blends. J Chem Eng Data 1998;43(3):378–82.
[54] Weiland RH. Carbon dioxide removal by mixtures of amines: Final report. Des Plaines: Gas Research Institute; 1996.
[55] Ying J, Eimer DA. Measurements and correlations of diffusivities of nitrous oxide and carbon dioxide in monoethanolamine + water by laminar liquid jet. Ind Eng Chem Res 2012;51(50):16517–24.
[56] Mangalapally HP, Hasse H. Pilot plant study of post-combustion carbon dioxide capture by reactive absorption: Methodology, comparison of different structured packings, and comprehensive results for monoethanolamine. Chem Eng Res Des 2011;89(8):1216–28.
[57] IEA Greenhouse Gas R&D Programme. CO_2 capture at gas fired power plants. Cheltenham: IEA Environmental Projects, Ltd.; 2012 Jul.
[58] Whitman WG. The two film theory of gas absorption. Int J Heat Mass Tran 1962;5(5):429–33.
[59] Razi N, Svendsen HF, Bolland O. Validation of mass transfer correlations for CO_2 absorption with MEA using pilot data. Int J Greenh Gas Con 2013;19:478–91.
[60] Billet R, Schultes M. Predicting mass transfer in packed columns. Chem Eng Technol 1993;16(1):1–9.
[61] Tsai RE, Seibert AF, Eldridge RB, Rochelle GT. A dimensionless model for predicting the mass-transfer area of structured packing. AIChE J 2011;57(5):1173–84.
[62] Chilton TH, Colburn AP. Mass transfer (absorption) coefficients prediction from data on heat transfer and fluid friction. Ind Eng Chem 1934;26(11):1183–7.
[63] Towler G, Sinnott RK. Chemical engineering design: Principles, practice and economics of plant and process design. 2nd ed. Oxford: Butterworth-Heinemann; 2012.
[64] Sinnott RK, Towler G. Chemical engineering design. 5th ed. Oxford: Butterworth-Heinemann; 2009.
[65] Strigle RF. Random packings and packed towers: Design and applications. 2nd ed. Houston: Gulf Publishing Company; 1994.
[66] Canepa R, Wang M, Biliyok C, Satta A. Thermodynamic analysis of combined cycle gas turbine power plant with post-combustion CO_2 capture and exhaust gas recirculation. P I Mech Eng E–J Pro 2013;227(2):89–105.
[67] Hoek PJ. Large and small scale liquid maldistribution in a packed column [dissertation]. Delft: Delft University of Technology; 1983.